Field Emission Displays (FEDs) and Surface-Conduction Electron-Emitter Displays (SEDs)

Matthew T. Cole[1], Masayuki Nakamoto[2] and William I. Milne[3]
[1]*Cambridge University, Cambridge, UK*
[2]*Shizuoka University, Shizuoka, Japan*
[3]*Cambridge University, Cambridge, UK*

1 Electron Emission: Field, Thermionic, and Photo

Excluding the transistor, the cathode ray tube (CRT) is perhaps one of the most important technological achievements of the past century. Indeed, very few people have not interacted with these displays at some point or another in their lives. These low-cost, simple displays pervaded almost every facet of society, industry, and commerce and accompanied the rapid development of the microprocessor and personal computing. Indeed, it is such displays that facilitate user–computer interaction. However, the relatively recent advent of ever more powerful and miniaturized processors has required the development of similarly portable and energy efficient display technologies, criteria that bulky, power-hungry CRTs no longer fulfilled. New technologies were necessary and the flat panel display market was spawned as a consequence. After an exponential growth between 1985 and 1995 [1], today, the flat panel display has an estimated net worth in excess of $135 billion per annum – one of the largest global markets in human history.

Electrons can be emitted from a solid in a number of ways. The most notable being field, thermionic, and photoemissions. Thermionic and photoemissions occur when electrons are thermally or optically excited, by external laser irradiation or Joule heating, for example, allowing them to become sufficiently energetic such that they pass over the emitting materials surface potential barrier. It is in this feature that field emission dramatically differs. Field emission is defined as *the emission of electrons from the surface of a condensed phase, electron-rich*

Handbook of Digital Imaging, Online © 2015 John Wiley & Sons, Ltd.
This article is © 2015 John Wiley & Sons, Ltd.
This article was published in the *Handbook of Digital Imaging* in 2015 by John Wiley & Sons, Ltd.
DOI: 10.1002/9781118798706.hdi023

surface, into a separate electron-deficient phase, usually a vacuum, under the influence of large electric field [2]. This phenomenon deals with quantum mechanical tunneling of energetically unexcited electrons through a deformed, nominally triangular potential barrier at a metal–vacuum interface. Field emission occurs at room temperature, and the emitters are commonly referred to as "*cold cathodes*." The intense electric fields profoundly augment the interface barrier, narrowing it to just a few tens of atoms. The extreme narrowness of the barrier permits an exponential tunneling of the local electron population through, rather than over, the confining potential barrier, an effect characterized by an extremely fast on–off time (<50 μs) [3].

In the case of thermionic emitters, found historically to pervade the display industry in the form of the CRT display, the emission current, work function ($\phi = 4{-}5$ eV), and operational temperature are intimately related [2]. Sti mulation of appreciable currents requires temperatures in excess of 1700°K. As a result, thermionic sources are energetically demanding, and the high operational temperatures induce severe emitter instabilities over time. The emitted electron beam also has extremely poor transient behavior as the on–off time can be of the order of a few seconds or more.

Photoemission occurs when an electron is excited into a higher energy state, greater than the vacuum level, as a result of incident radiation of a suitable wavelength, v. It occurs when surfaces are irradiated with photons of energy $hv \geq \phi$, where h is Planck's constant (6.626×10^{-34} J s) [2]. For most metallic emitters, this threshold wavelength is in the visible or ultraviolet region. A major drawback, which confines photoemission to the laboratory bench top rather than the commercial arena, is that it is difficult to stimulate significant emission currents. Electrons are only liberated from the emitter's surface, and much of the incident irradiation is reflected. Moreover, the energy of the excited electrons is readily absorbed and redistributed within the emitter bulk due to the likely interactions with the conduction electrons. Photoemission is also known for its relatively high noise component, as ambient light induces chaotic emission [4].

Field emission sources have a number of attractive features. In addition to their room temperature operation, they respond nearly instantaneously to field variations, have high tolerance to temperature fluctuations and incident radiation, and have a high degree of focusability, large on/off ratios, highly nonlinear emission characteristics, and high emission current densities of the order of amperes [5].

2 Field Emission Theory

Field emission is a wholly quantum mechanical phenomenon and can be succinctly described in adequate detail using fairly simplistic descriptions based on the free-electron model. In its simplest form, the current density (as a function of the applied electric field), $J(F)$, is given by

$$J(F) = \left(\frac{A}{\phi t^2(s)}\right) F^2 \exp\left(-Bv(s)\frac{\phi^{3/2}}{F}\right), \tag{1}$$

where $A = (e^3/8\pi h) = 1.54 \times 10^{-6}$ A eV V^{-2} and $B = (8\pi/3eh)(2m)^{1/2} = 6.83 \times 10^9 (\text{eV})^{-3/2}$ V/m, and $t(s)$; $v(s)$ are the purely mathematical slowly varying dimensionless

Handbook of Digital Imaging, Online © 2015 John Wiley & Sons, Ltd.
This article is © 2015 John Wiley & Sons, Ltd.
This article was published in the *Handbook of Digital Imaging* in 2015 by John Wiley & Sons, Ltd.
DOI: 10.1002/9781118798706.hdi023

Nordheim elliptic functions [6, 7] and are approximated by

$$t(s) = \frac{(3.79 \times 10^{-5})F^{1/2}}{\phi}; \tag{2}$$

$$v(s) = (0.956 - 1.062s^2). \tag{3}$$

ϕ denotes the work function of the emitting material. For simplicity, $v(s)$ is most often set to unity with negligible loss in accuracy. A rather elegant modification to Equation 1 was proposed by Brodie and Spindt [8] to form a more tractable description. By substituting the current density and emission area with the measured current (I) and the local electric field with the product of the applied bias (V) and a cathode geometry-dependent field factor, they concluded that

$$I = V^2\beta^2 \left(\frac{A^*A}{\phi\delta^2}\right) \exp\left(\frac{-B\phi^{3/2}\delta}{\beta V}\right). \tag{4}$$

Here A^* is the effective emission area, δ the constant anode electrode separation, and β the field enhancement factor, which is proportional to the aspect ratio of the emitting surface and is given by

$$\beta = \frac{F_{\text{local}}}{F}, \tag{5}$$

where F_{local} is the apex-enhanced electric field. The field enhancement factor β is a standard performance metric that is empirically evaluated for any given emitter by measuring the current–voltage (I–V) characteristics and plotting a so-called Fowler–Nordheim curve of the form

$$y = mx + c \Rightarrow \ln\left(\frac{I}{V^2}\right) = \left(\frac{-B\phi^{3/2}\delta}{\beta}\right)\frac{1}{V} + \ln\left(\frac{A^*A\beta^2}{\phi\delta^2}\right). \tag{6}$$

β can then be calculated from the gradient of the linear (I/V^2) versus ($1/V$) plot, where the bracketed terms are all known constants:

$$\frac{\mathrm{d}y}{\mathrm{d}x} = \frac{\mathrm{d}(I/V^2)}{\mathrm{d}(1/V)} = \frac{-1}{\beta}(B\phi^{3/2}\delta). \tag{7}$$

Similarly, the y-intercept of Equation 7 can be used to determine either the work function or the effective emission area if necessary. Figure 1b shows typical $I - V$ and Fowler–Nordheim characteristics of an array of W nanowires [10]. To obtain stable performance, vacuums of 10^{-9}–10^{-7} mbar are required to avoid tip damage by gas ionization and ion bombardment.

β is strongly related to the emitter morphology. Thus, it can also be determined using electron microscopy to assess the emitter's aspect ratio. This dependence was illustrated through the theoretical work of Rohrbach [11] and is summarized in Figure 2. Extremely narrow, elongated emitters are preferred as they enhance the local field and, therefore, turn-on at lower local electric fields compared to short and stubby emitters.

The turn-on field and threshold field are widely used performance metrics but are unfortunately less well defined. High performance emitters have low turn-on and low threshold fields. The former classically refers to the field necessary to emit 1 nA/cm^2, while the latter refers to the field required to yield a current density of the order of 10 mA/cm^2 [12]. For clean metallic

Handbook of Digital Imaging, Online © 2015 John Wiley & Sons, Ltd.
This article is © 2015 John Wiley & Sons, Ltd.
This article was published in the *Handbook of Digital Imaging* in 2015 by John Wiley & Sons, Ltd.
DOI: 10.1002/9781118798706.hdi023

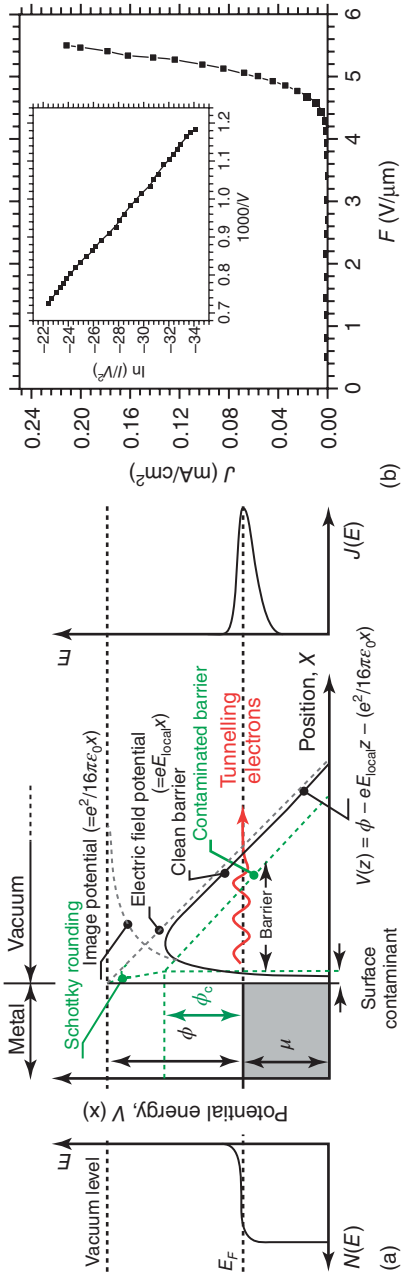

Figure 1 (a) Field emission potential diagram. Large electric fields induce barrier narrowing, which increases the number of electrons tunnelling from the Fermi level in the metallic, electron-rich, surface into the vacuum. Variations in density of occupied states, $N(E)$, and current density, $J(E)$, as a function of electron energy. Surface contamination and charging effects (Schottky rounding) can be seen to drastically alter the potential profile. Adapted from Refs 4, 9. (b) Example J–F characteristics for an array of W nanowires and the corresponding (inset) Fowler–Nordheim plot [10]

Handbook of Digital Imaging, Online © 2015 John Wiley & Sons, Ltd.
This article is © 2015 John Wiley & Sons, Ltd.
This article was published in the *Handbook of Digital Imaging* in 2015 by John Wiley & Sons, Ltd.
DOI: 10.1002/9781118798706.hdi023

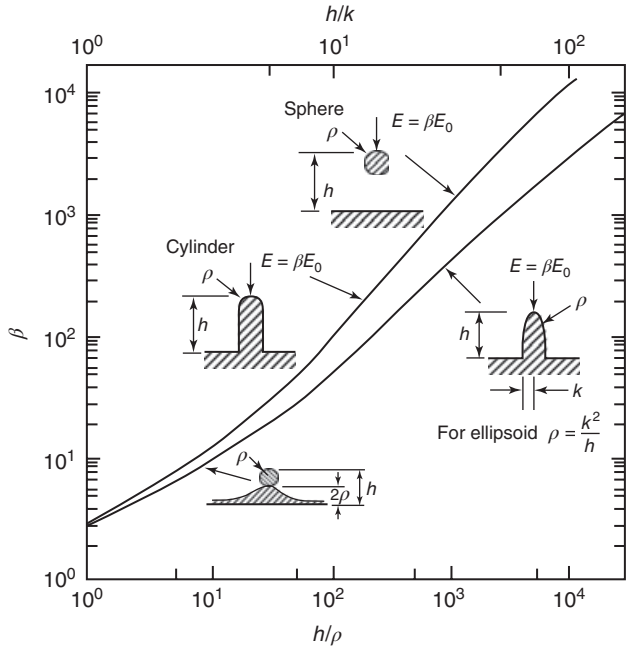

Figure 2 Field enhancement factors (β) for various idealized emitter geometries including surface contacted and suspended spheres, in addition to hemispherical and ellipsoidal topped cylinders [11]

surfaces, electrons are emitted when the barrier width is reduced to a few nanometers under electric fields of the order of 5 kV/μm. This typically results in a current density of around 10^2–10^3 mA/cm^2.

We have, in the models presented until this point, only considered ideal potential barriers at the interface between a perfect conductor and a perfect vacuum. In reality, these surfaces are contaminated with a variety of undesirable absorbates, such as H_2O, which is absorbed during emitter wet-etching, for example. Such coatings adjust the profile of the surface barrier. Figure 1a shows the effect of an electropositive contaminant on the barrier profile. Note that the use of the Richardson's composite ϕ in all of the preceding models does not provide a suitable account of the barrier modification – rather a full consideration of the augmented potential profile is necessary. Another subtle deviation from this ideal triangular barrier comes in the form of Schottky rounding at the barrier peak. Here, the top of the potential is smoothed by charge image effect and results in a 10–20% reduction in F for a given emission current [4]. Schottky rounding is largely unimportant in modeling strong field emission at ordinary emission temperatures [13]. A further *image potential* is also known to modestly adjust the effective barrier [14], as shown in Figure 1a. The theory of field emission from semiconducting materials has not been considered here and is beyond the scope of this section due to their typically poor emission characteristics.

In order to extract high currents, either the electric field must be increased or, as mentioned previously, the work function decreased. The local electric field can be increased by engineering high β emitters, as shown by Utsumi [15]. We are limited in the range over which we

Handbook of Digital Imaging, Online © 2015 John Wiley & Sons, Ltd.
This article is © 2015 John Wiley & Sons, Ltd.
This article was published in the *Handbook of Digital Imaging* in 2015 by John Wiley & Sons, Ltd.
DOI: 10.1002/9781118798706.hdi023

can reduce ϕ. Low ϕ materials tend to have low melting temperatures and undergo significant deformation under the influence of high electric fields. Emitter deformation augments the local electric field and induces run-away degradation. In practice, a combination of β enhancement and ϕ reduction is used. This is achieved by fabricating sharp pyramids, Spindt tips, or columns made from polycrystalline refractory metals such as W (4.5 eV) and Mo (4.7 eV), while using low ϕ alkali metal coatings, such as Cs (1.9 eV), Ba (2.3 eV), or ZrO (2.3 eV). These coated, or Schottky-type emitters, not only offer the advantages discussed earlier but also reduce the kinetic energy spread of the liberated electrons, defined as the full-width half maximum of the energy spectrum [$J(E)$ versus E], to ~0.3 eV and the corresponding virtual source size – the effective width of the emitted electron beam – to around 15 nm. Small energy spreads and narrow virtual sources are desirable as they increase image sharpness, contrast, and on/off switching speeds. Schottky emitters are brighter (10^8 A cm^{-2} SR^{-1}) than W emitters and have a typical temporal stability (i.e., the degree of variation in the emitted current with time) of <1%. Substantial continuous-operation lifetimes are also not uncommon (1–2 years). Unfortunately, the noise level of Schottky emitters tends to increase with time. Despite this, Schottky emitters have the best lifetime characteristics of all emitters. The ϕ-lowering Zr readily evaporates when exposed to vacuum and is rapidly replaced from the Zr reservoir within the W bulk. This gives rise to relatively stable emission characteristics.

Uncoated W emitters have small virtual source sizes (~3 nm) and room temperature functionality. The emission stability, however, can vary by as much as 6%. W has a strong affinity toward water, which is necessary during the tip-forming etch process. Unfortunately, water is readily absorbed and desorbed under modest heating. This varies the emitter work function uncontrollably, which induces thermal instabilities. The stability issue is further exacerbated as, when exposed to high electric fields, the metallic bonds, which are generally weaker than covalent bonds found in many carbon allotropes for example, permit significant atomic diffusion within the W tip. This electromigration, over time, changes the shape of the tip. This augments the local electric field profile, giving rise to current oscillations, inhibited functionality, and a positive-feedback tip degradation. It is important to note that, although field emission is, in principle, a room temperature process if high currents are extracted, tip heating is not uncommon, and it is this heating that is often the cause of tip degradation.

3 The History of Field Emission Displays: Laboratory to Market

Thermionic emission was first reported in 1873 by F. Guthrie [16, 17] who noted that heated objects readily lose their charge. H. Hertz, in 1887, similarly observed that electrons could be liberated by irradiating various materials with light of particular wavelengths [18]. During the advent of the X-ray tube and valve technologies in the 1920s, unexpected electron emission was observed at room temperature. The Marconi Company noted, during the first intercontinental radio broadcasts, electric arcs in the radio equipment's vacuum tubes. Careful analysis revealed that these arcs had a tendency to occur at rather specific surface protrusions, bumps, and whiskers on the tungsten filaments – although the details of the process remained a mystery. The measured arcing characteristics were highly unstable and were believed at the time to be attributed to room temperature thermionic emission enhanced by the Schottky effect. Speculation was rife. However, as vacuum techniques developed, increased amounts of reliable empirical data became available, and it was soon realized that the observations and proposed model were inconsistent.

Handbook of Digital Imaging, Online © 2015 John Wiley & Sons, Ltd.
This article is © 2015 John Wiley & Sons, Ltd.
This article was published in the *Handbook of Digital Imaging* in 2015 by John Wiley & Sons, Ltd.
DOI: 10.1002/9781118798706.hdi023

In the 1920s, R. Fowler and L. Nordheim, then at the Cavendish laboratory, Cambridge University, realized that the emission mechanism was profoundly different from traditional thermionic and photostimulation [13]. The then recent ground breaking work of P. Dirac, E. Schrödinger, and W. Pauli on quantum mechanics was to become the inevitable vehicle for the renowned Fowler–Nordheim breakthrough. Fowler and Nordheim, following the theoretical work of Lauritsen and Oppenheimer on Millikan's experiments, realized that the emission process was purely quantum mechanical in nature and that accurate consideration of the electrons wave functions could account for the observed emission characteristics, with rather high degrees of accuracy. The theory of field emission was born; however, it took almost a decade of empirical studies until it was independently verified by E. Müller, who, in 1936, successfully grew and characterized monocrystalline electron emitting tips. Unbeknown to Műller at the time, he had also rather unwittingly just invented the first field emission electron microscope capable of atomically resolving the emitter's crystalline structure.

Until this point, repeatable field emission was only achieved using individual tips that had been chemically etched into sharp points, a few hundred nanometers in diameter. Even at these diameters, a few thousand volts were still required to stimulate suitably large emission currents. The problem, although deceivingly simple, was in fact a major hurdle: How does one go about inducing large currents whilet using a low voltage source? Micro- and nanofabrication techniques advanced rapidly in the early 1940s and 1950s and offered a viable means to position electrodes and tips extremely close to one another, significantly closer than had previously been possible. Microfabrication also paved the way to the fabrication of exceptionally narrow, submicron diameter tips. Massive tip parallelization was also then practical using photolithographic techniques. All of these factors led to an increase in field concentration at the tip and, hence, a reduction in the extraction voltage. Extraction voltages were then a hundred volts or so making, for the first time, display applications commercially viable. The thermionic emitting CRT, at that time, dominated the display market and had no serious competitors. However, many realized that replacing the power-hungry thermionic source with a field emission source would lead to displays that were thinner, flatter, lighter, and much more energy efficient.

In 1968, K. Shoulders and C. Spindt envisaged the fabrication of a field emission flat panel display for the first time using arrays of microscopic Mo tips. Spindt proposed a combination of polycrystalline metal thin films, physical vapor deposition, and etching techniques twinned with high resolution photolithography and electron beam lithography to form arrays of conical emitters [19]. Combined with matrix addressing, they had come up with the fundamental elements for the field emission display (FED). Figure 3 depicts the structure of a standard FED and, for comparison, the structure of a CRT. A number of similarities are clear. For example, the necessity for a high interelectrode vacuum, an electron source, and the light emitting RGB (red/green/blue) phosphors is consistent between the two. However, FEDs are compact and lightweight. Moreover, the image is formed from thousands of simultaneously firing electron emitters rather than only a few beams (typically three), as in the case of a color CRT. In an FED, the extraction potential is selectively applied on bus-like electrodes to address individual subpixels. This applies a local potential between the sharp emitting structures – tips, Spindts, or more modern nanomaterials – and the extraction anode, which induces electron emission. These electrons are then focused by the gate electrode toward the appropriate RGB phosphor to form a single pixel. Each pixel is made up of a red, green, or blue subpixel and is of the order of 50 μm in size. Pixels on the submicron scale are possible, facilitating ultrahigh resolution displays with pixel densities far in excess of the HDTVs that are available today.

Handbook of Digital Imaging, Online © 2015 John Wiley & Sons, Ltd.
This article is © 2015 John Wiley & Sons, Ltd.
This article was published in the *Handbook of Digital Imaging* in 2015 by John Wiley & Sons, Ltd.
DOI: 10.1002/9781118798706.hdi023

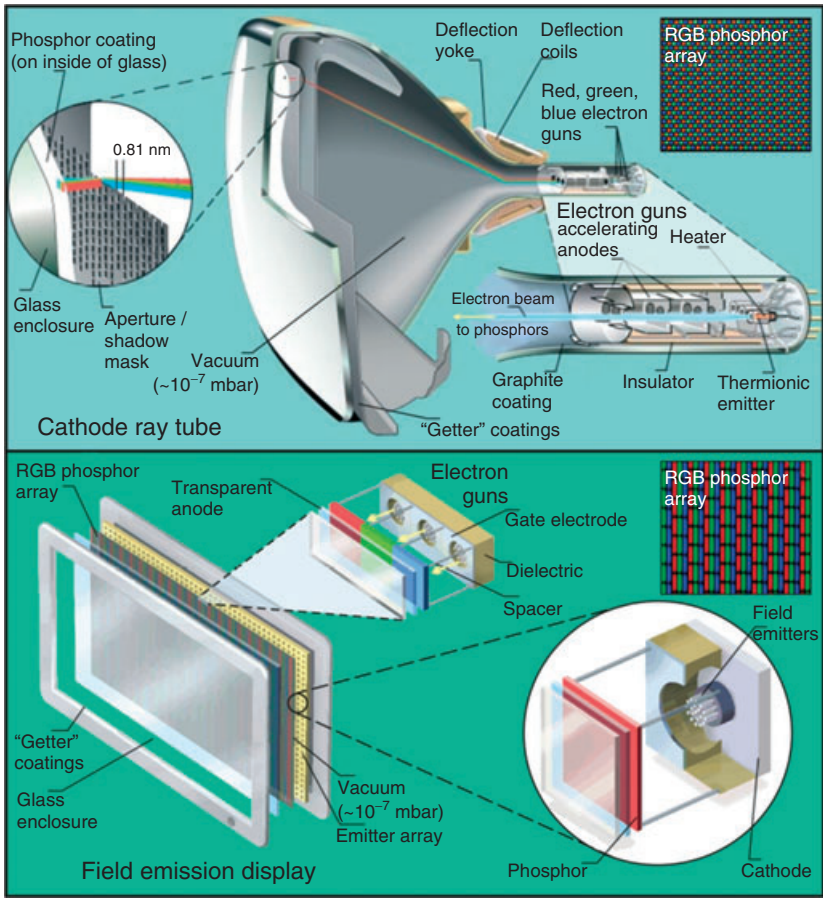

Figure 3 Structure of an FED compared with the more traditional CRT display. Obvious benefits of FEDs include substantially thinner and lightweight displays, higher energy efficiency by removing the thermionic electron source, simplified planar construction, thousands (rather than three) of simultaneously firing electron beams, rapid subpixel switching rates (<1 ms), wide viewing angles (160°), and high contrast ratios. The reduction in cavity volume also improves the quality of the vacuum and, therefore, display lifetime and stability. The *insets* show typical RGB phosphor masks for each technology. Adapted from Refs 20, 21

As with all display technologies, the data bus largely dictates the ultimate image resolution to some extent, although, perhaps, more of an issue for FEDs in particular is the noisy process of electron emission. Field emission is intrinsically a noisy process. Many tens of emitters firing collectively are required to smooth out this randomness. The development of extremely morphologically uniform emitters will result in significant noise reduction; however, with further miniaturization (necessary to increase display efficiency) comes enhanced noise levels. Conversely, there seems to be no limit on the maximum pixel size. Indeed, centimeter-scale FED light sources have been fabricated, which are, in essence, single-pixel displays. An extremely wide color gamut can be produced by controllably mixing the optical emission from the RGB

Handbook of Digital Imaging, Online © 2015 John Wiley & Sons, Ltd.
This article is © 2015 John Wiley & Sons, Ltd.
This article was published in the *Handbook of Digital Imaging* in 2015 by John Wiley & Sons, Ltd.
DOI: 10.1002/9781118798706.hdi023

phosphors by exciting multiple phosphors at once with precise beam currents. High currents stimulate an intense optical emission, while lower currents give rise to subtler hues. For display applications, current densities of ~5 mA/cm^2 are typically required [12].

At the time of publishing, liquid crystal displays (LCDs) dominated the display market. They require backlighting while FEDs do not. This significantly adds to the power consumption of LCDs as the backlight is always "on." Moreover, a vast proportion of the light is typically lost via the necessary optical polarization and color filtering. LCDs typically consume around 100 W, whereas electron emission displays are around 10 times more efficient. Perhaps, the main feature dictating the fundamental limit on power efficiency of FEDs is the phosphor efficiency. Next-generation phosphors that offer equivalent luminance at lower current exposures will ultimately improve FED performance further. LED displays, and their variants, although not requiring any external backlighting or color filters, are still relatively inefficient and are comparable in efficiency to LCDs. Nevertheless, highly efficient LEDs are being hastily developed to increase competitiveness. Plasma display panels have the lowest lifetime and lowest efficiency (typical consumption: 200–300 W). Image degradation by burn-in also plagues plasma displays.

The more rapidly the display can respond to its drive signal, the better the image fidelity to fast moving images. This reduces image blurring and smearing. The typical response time of FEDs is less than 1 ms. Indeed, response times <50 μs have been reported [3]. LCDs have slower response times of between 5 and 20 ms, whereas LED displays respond between 4 and 25 ms. Plasma displays function by exciting a UV plasma within each subpixel, which stimulates UV-active RGB phosphors. This process is very fast and typically occurs within less than 1 ms.

Returning to FEDs, a major challenge in emitter fabrication was in achieving sharp tips. The sharper the tip, the higher the geometrical field enhancement and the lower the drive voltages. A reduction in the drive voltage was a commercial necessity. Reducing the drive voltage meant a reduction in the physical size of the voltage supply. Voltage supply reduction was critical as it was this incumbent feature that contributed toward most of the displays weight and power consumption. A number of solutions were developed, with varying degrees of success. The most effective was that proposed by J. D. Levine who, in the early 1970s, found that, when the oxide of a natively oxidized Cu tip was etched away an exceptionally fine tip, only a few atoms in diameter, remained. However, severe electromigration and stability issues associated with Cu prevented further development of the approach. Nonetheless, Levine had made an important contribution to the processing history of field emission tips and tip sharpening through selective oxide removal.

During these embryonic stages of tip manufacturing, the extraction and gate potentials were of the order of 1000–4000 V. These driving potentials were too high for realizable devices and resulted in multiple arcing and trapped gas ionization events that damage the emitters. The local tip environments were extremely aggressive, and few tips lasted for any appreciable length of time. Certainly, none survived long enough to permit commercialization of the technology. The need for improved vacuum-forming techniques was apparent. High voltages, those in excess of 6 kV, were also found to be especially inappropriate as X-rays were generated as the incident beams irradiated the W getters necessary to maintain the vacuum. A resolute effort to fabricate even smaller and sharper tips was made in addition to placing the extraction electrode much closer to the driven electrode to provide a switching potential of ~10 V. Switching losses must be minimized.

Handbook of Digital Imaging, Online © 2015 John Wiley & Sons, Ltd.
This article is © 2015 John Wiley & Sons, Ltd.
This article was published in the *Handbook of Digital Imaging* in 2015 by John Wiley & Sons, Ltd.
DOI: 10.1002/9781118798706.hdi023

By the early 1970s, silicon-processing techniques and infrastructure had developed to the point that many researchers were interested in using Si rather than Mo tips. Indeed, a number of the oxidation techniques developed for polycrystalline metallic emitters were based on techniques and processes previously used to fabricate the original semiconductor-based emitters. Williams and Simon investigated field emission from forward biased GaAs $p-n$ junctions coated with Cs and O. Suitable coating gave rise to an effective negative electron affinity at the vacuum interface [22]. They believed that the electrons, in the extremely narrowed depletion layer, would reside in an extremely high electric field region and could, therefore, gain the necessary kinetic energy to propagate to the emitters' surface and overcome the work function and emit into the vacuum. Although they were proven correct, their rather interesting platform had extremely poor efficiencies, and as a consequence, no FEDs based on their ideas were developed.

A paradigm shift in fabrication occurred in 1995. D. Hsu deviated from the more traditional top–down etching techniques used thus far. Techniques based on bottom-up growth were considered. This change was an indication of things to come. Chemical vapor deposition (CVD) was used to fabricate Pt/Li/Pt composite thin film edge emitters that were free standing, triangular in shape, and very sharp. Si-based emitters soon became outdated owing to their poor performance and demanding and often prohibitively costly fabrication, with some displays requiring over 250 processes to form the final FED, the majority of which were associated with the etching and defining of the Si tips. Concurrently, other materials were beginning to be investigated as suitable cold cathode emitters. The only requirements being that the material was suitably conductive and could be processed into high aspect ratio geometries. Mo, W, Ni, Pt, Ir, C, and conductive carbides were some of those investigated. Figure 4 shows the emission characteristics of some of these various materials.

Baker, Williams and Osborn [32], in 1972, had noticed that, in various environments, the emitted current from graphite fibers was extremely stable. Wang *et al*. [33] and Geis *et al*. [34], in 1991, using diamond-based cathodes, reported the onset of emission at surprisingly low threshold fields (<3 V/μm). Djubua and Chubun [35], that same year, confirmed that arrays of diamond-like carbon (DLC) cones emitted at extraction potentials much less than those of Mo or Hf. Clearly, carbon, as it seemed, was the material of choice for the next generation of field emitters. Rather surprisingly, even though significant amounts of intellectual property were developed, no displays based on these concepts were developed, most likely because of a number of processing difficulties associated with the diamond derivatives and poor understanding of the materials' growth mechanisms. Nevertheless, carbon had been shown to have exceptional field emission properties, and in the late 1990s and early 2000s carbon-based field emitters resurged into prominence through the discovery and exploitation of a new high aspect ratio carbon allotrope – the carbon nanotube (CNT), an important material, which we will discuss later.

In 1985, the Stanford Research Institute was one of the first to successfully demonstrate a prototype monochromatic FED. Only 2 years later, a full color FED using arrays of 1-μm Mo tips was presented. The year 1991 saw the release of Candescent's thin CRT displays, which were also based on Mo Spindt technology. These initial displays solved many important engineering problems, particularly those related to vacuum maintenance, and stimulated the field. FEDs were becoming increasingly viable. Nonetheless, a number of important engineering challenges remained. The inevitable lateral velocity of the emitted electrons resulted in unacceptable beam divergence and image blurring. This is the case for all field emitters,

Handbook of Digital Imaging, Online © 2015 John Wiley & Sons, Ltd.
This article is © 2015 John Wiley & Sons, Ltd.
This article was published in the *Handbook of Digital Imaging* in 2015 by John Wiley & Sons, Ltd.
DOI: 10.1002/9781118798706.hdi023

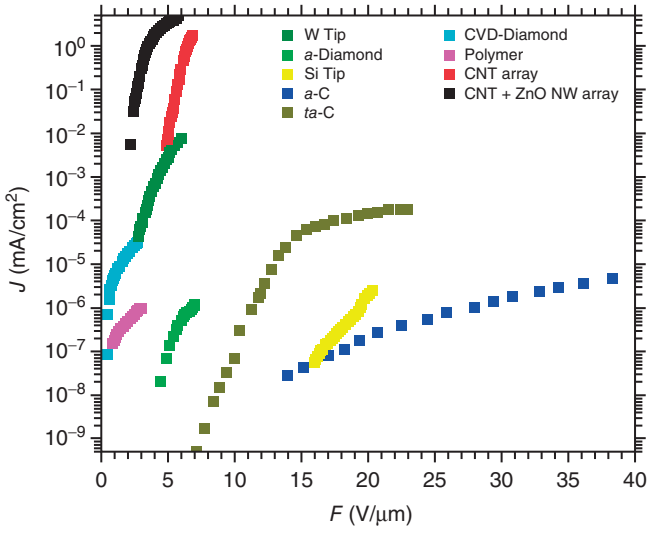

Figure 4 Field emission characteristics of various materials, including W tip nanoarrays [23], amorphous (*a*-) diamond [24], Si tips [25], *a*-carbon [26], tetrahedral *a*-carbon [27], chemical vapor-deposited diamond [28], regioregular poly(3-octylthiophene) polymer [29], a carbon nanotube array [30, 31], and a zinc oxide nanowire-coated carbon nanotube array [30]. *Source*: Reproduced with permission from Ref. 20. © IEEE, 2003

regardless of the sharpness of the tip. Integrated electrooptics, in the form of gate electrodes, were and still are necessary. The emission characteristics were also highly dependent on the emitter geometry. Slight geometric variation induced major disparities between the emission characteristics of adjacent emitters. Consequently, ballasting films – essentially current limiting resistors – had to be integrated to increase display uniformity. This propensity for single tip dominance, overemission, and consequent burn-out, in arrays or in whisker-like nanomaterial composites, still plagues FED manufacturers today. The solution, it was thought, to this tip erosion was to reduce the accelerating voltages.

Despite these problems, FED development continued [36], and although field emission was becoming increasingly viable as a commercial technology, the ongoing problem of poor vacuum, high voltage drivers, and the lack of efficient low voltage phosphors continues. Until this point, the inefficient phosphors developed for CRTs had been used, and new low voltage, bright variants were required. These technological difficulties were soon joined with a downturn in the commercial landscape. LCDs were undergoing the final stages of aggressive commercialization. They operated at much lower voltages than the FEDs of the time. This made them extremely attractive. Their relatively low power and efficient operation offered incredible competitiveness, especially for portable applications in the burgeoning laptop market. Nonetheless, the wide-viewing angle of FEDs, general inertness to temperature variations, high contrast ratio, and extreme slim-line design maintained the feasibility of the technology.

By 1994, Micron Display had, for some time, been making a concentrated effort to develop a new tip fabrication technique based on chemical mechanical polishing; a process that obviated many time-consuming and expensive lithographic processes. Prefabricated tip arrays were

Handbook of Digital Imaging, Online © 2015 John Wiley & Sons, Ltd.
This article is © 2015 John Wiley & Sons, Ltd.
This article was published in the *Handbook of Digital Imaging* in 2015 by John Wiley & Sons, Ltd.
DOI: 10.1002/9781118798706.hdi023

coated with a dielectric/conductor bilayer. Tips were then polished to reveal the extremely sharp emitter with the conductive layer functioning as the gate electrode. The technology was finally released in 1996 in the form of a 0.55-in. military viewfinder and thermal imager for handheld weapons applications. At a similar time, Futaba commenced full-scale pilot production of a 5.2-in. ¼ VGA monochromatic ZnO:Zn phosphor FED developed primarily for the avionics industry. PixTech also began large-scale production at this time, producing displays consisting of 2000, 1.2-μm tall Mo tips per pixel operating at anode and gate potentials of 350 and 80 V, respectively [36]. A large number of emitters per pixel were necessary to produce uniform brightness. As mentioned previously, field emission is intrinsically noisy, and large numbers of emitters statistically reduce this inherent noise. PixTech, in 1996, released a 10.5-in. full color FED and other extremely bright FEDs capable of unprecedentedly wide-viewing angles (160°), while, soon after, Sony released their FED portable DVD platform (Figure 5b). Sony was becoming a major player. Partnering with Candescent, in 1998, Sony publicly announced the opening of a new production facility in the United States. However, this encouraging statement was short-lived when, in late 2004, these assets were sold to Canon. Despite this, by 2008, Sony had heavily developed its nano-Spindt technology and had successfully developed full color 26-in. FEDs with the aim of mass producing 60-in. displays by 2015 (Figure 5c) [40].[1] At this time, getters, deliberately deposited reactive metals such as Mo and W that readily absorb and chemically bond to free gas molecules in the display cavity used to maintain the vacuum, were continuing to be developed to resolve the ongoing vacuum issues – a design feature that was becoming increasingly problematic as displays continued to upsize.

The latter half of these major developments (based on the then standardized Spindt technology) were accompanied, in 2000, by a substantial shift toward the use of carbon-based nanomaterials. The early seminal work of Baker, Williams and Osborn [32] and others

Figure 5 Traditional Spindt-type emitters. (a) Cross-section schematic of a typical field emission display (Courtesy of Pixtech). The red, green, and blue phosphors are excited by the field emitted electrons liberated from the sharp tips. A scanning electron micrograph of a single Si Spindt [37]. (b) A Sony portable DVD player using a Candescent FED (Courtesy of C. Curtin and K. L. Jense, "Theory and Simulation of field emission from microstructures", http://other.nrl.navy.mil/CREBWorkShop/Jensen.pdf). (c) Sony's 26-in. FED released in 2008[1]. (d) Samsung's 15-in. 840 × 480 pixel FED [38, 39]. The *inset* shows a scanning electron micrograph of etched Si Spindts. *Source*: Reproduced with permission from Ref. 5. © Allied Publishing LLC, 2004

[1] Sony's field emission company wants to roll out 60-in. FED-TVs.

Handbook of Digital Imaging, Online © 2015 John Wiley & Sons, Ltd.
This article is © 2015 John Wiley & Sons, Ltd.
This article was published in the *Handbook of Digital Imaging* in 2015 by John Wiley & Sons, Ltd.
DOI: 10.1002/9781118798706.hdi023

[21, 26, 27] split the wide variety of carbon materials, previously discussed, into two distinct groups based on their proposed emission mechanism. These were the structured graphites (sp^2 bonded), where the emission was a result of field enhancement of the conductive emitter, and the diamond types (sp^3 bonded), where negative electron affinity [41–43] and band bending effects [44, 45] were thought to be important. At that time, wide bandgap materials, such as diamond and its synthetic derivatives, were believed to have a low or even negative electron affinity. Electrons injected into the conduction band observe a reduced potential barrier and, as a result, easily emitted into vacuum. For carbon emitters, it is now widely accepted that this is not the case. In principle, such band bending effects would apply homogeneously over the emitters' entire surface, resulting in spatially uniform emission. Yet, the observed field emission repeatedly occurred at a few highly localized and randomly distributed sites. The widely accepted model and data were inconsistent. Spatial mapping of the field emission characteristics hinted that there was something peculiar about the emission sites in relation to the rest of the planar carbon coatings [46]. It soon became clear that the field enhancing characteristics originated from the graphitic grain boundaries [47], which coincided with arcing sites, a result largely supported by the fact that highly defective and interface-rich films exhibited superior field emission properties compared to uniform films. As an example, the emission performance of tetrahedral amorphous carbon (*ta*-C), an extremely uniform thin film, was shown to dramatically improve after *activation*, that is, when a vacuum arc discharge event occurred between the emitter and the extraction electrode, with sufficient vigour to perturb the surface topography to form tip-like structures [48, 49]. The presence of crystallographically defective sp^2 regions (about 20%) in the otherwise highly crystalline sp^3 *ta*-C offered one such source of suitable activation sites for arcing.

A new trend emerged: the production of intentionally diverse composite carbon films, rich in a variety of graphitic nanostructures. These films contained incredible assortments of carbonaceous nanostructures, including, but certainly not limited to carbon, particles, onions, clusters, fullerenes, nanotubes, and nanofibers. These nanostructured carbon films performed significantly better than the leading carbon materials at that time, *ta*-C and DLC and the competing metallic emitters. These new nanostructured emitters had turn-on fields as low as 1–5 V/μm.

Field emission has been reported from CVD diamond [50], CVD graphite [51], nanostructured carbon [51, 52], and various polymers [29]. Motorola [53], in the late 1990s, investigated DLC-based FEDs [54, 55]. Of the emitting materials considered, those with the highest aspect ratios or particularly perturbed surfaces were found to outperform the smoother conformal coatings. Evidently, sharp tips were still preferred, even in the case of carbon-based emitters. Thus, the stage was set for the dramatic insertion and intense interest in CNT field emitters.

CNTs are one-dimensional carbon allotropes formed from cylindrically nested graphene sheets. They have diameters between 1 and 500 nm and lengths of up to several millimeters and are perfect candidates for field emission applications, including FEDs that could potentially, in the future, exploit the mechanical flexibility of these supramolecules. CNTs can be single- or multiwalled. Single-walled CNTs can be semiconducting or quasi-metallic depending on their chirality. Multiwalled CNTs (MWCNTs) are always metallic-like and are known to have a low axial resistance.

CNT deposition techniques have progressed rapidly in the past decade. CNTs can now be synthesized by a wide variety of methods, some more exotic than others, although all of which are broadly either sublimation or thermal decomposition process. The most common varieties include electric arc discharge [56–58], laser ablation [59–61], and thermal [62, 63] and

Handbook of Digital Imaging, Online © 2015 John Wiley & Sons, Ltd.
This article is © 2015 John Wiley & Sons, Ltd.
This article was published in the *Handbook of Digital Imaging* in 2015 by John Wiley & Sons, Ltd.
DOI: 10.1002/9781118798706.hdi023

plasma [64–66] CVDs from carbon-containing precursor gases. By virtue of their extremely strong sp^2 C–C bonding, intrinsic to the graphene hexagonal lattice, nanotubes have demonstrated impressive chemical inertness, unprecedented thermal stabilities, significant resistance to electromigration, and exceptionally high room temperature axial current density carrying capacities. These cold cathode electron emitters have incredibly high electric field enhancing aspect ratios combined with virtual point sources of the order of a few nanometers in size, making them near-ideal electron sources.

Extending the theoretical work of Rohrbach (Figure 2) [11], Utsumi [15] evaluated the shape of many commonly used field emission tips (Figure 6) and concluded that the best tips should be whisker-like. Evidently, CNTs fulfilled the Utsumi criterion perfectly. An additional important characteristic of nanotube emitters, compared to their metal counterparts, is associated with their temperature coefficient of resistance. Purcell *et al*. [73] demonstrated that MWCNT emitters can heat up to 2000°K as a result of the field emitted current but concluded more notably that the emission remains stable. Typically the resistance of a metal increases with temperature and an increase in channel resistance and further subsequent heating as increasing currents are. The combined elevated temperature and intense electric fields trigger tip field sharpening in metallic emitters. The metal passes its glass transition temperature and becomes increasingly fluid at such elevated temperatures and intense tip-localized fields, which tends to sharpen the tip. This positive feedback inevitably leads to emitter destruction as sharper tips pass higher currents, which induce further tip heating and sharpening. In contrast, the axial resistance of nanotubes decreases as they are heated. This limits the heat generation. In fact, the temperature coefficient of resistance for nanotubes varies sublinearly with current. Furthermore, graphite and nanotubes do not melt or flow. Rather they sublime, at extremely high temperatures approaching 2500°C. This further reduces the likelihood of thermally induced tip deformation [20]. These unique characteristics of nanotubes combine the benefits of planar graphite cathodes with the high aspect ratios of metal-tip technologies, allowing for lower operating potentials, simple and low cost bottom-up deposition and patterning, and large area processing.

In most applications today, nanotubes are first mass produced, purified, and mixed with an epoxy/binder, such as Teflon or Nafion, and then screen printed, cast, sprayed, or electrophoretically positioned. In these polymer–nanotube thin film composites, the polymer binders occlude much of the emitting surface and introduce substantial interfacial resistance. Pure CNT thin films have been successfully deposited onto various substrates using vacuum filtration, mechanical compression and shearing, direct growth, and physical extrusion techniques. However, reduced surface adhesion limits the usefulness of many of these techniques. Poor alignment in such films, which are in fact dense percolation networks, did not significantly limit the relatively impressive field emission performance compared to the proceeding metal emitters. Even curly "spaghetti-like" nanotube networks have been show to vertically align under the application of an electric field (>5 V/μm), thereby forming high quality field emission whisker-like structures [74].

Samsung were the industry leader on the development of CNT-based FEDs for some time. Figure 7b shows a 4.5-in. prototype FED based on CNT thin film technology. In the early 2000s, Samsung unveiled a 38-in. full color FED TV using unaligned CNT thin films [78]. Philips, Teco Nanotech, Co., and ISE Electronics have all worked on the development of CNT-based FEDs. Teco Nanotech, Co., marketed three basic CNT-based FEDs, the largest of which is 8.9 in. J. Dijon, at CEA-Leti in Grenoble, in 2005, reported the development of

Handbook of Digital Imaging, Online © 2015 John Wiley & Sons, Ltd.
This article is © 2015 John Wiley & Sons, Ltd.
This article was published in the *Handbook of Digital Imaging* in 2015 by John Wiley & Sons, Ltd.
DOI: 10.1002/9781118798706.hdi023

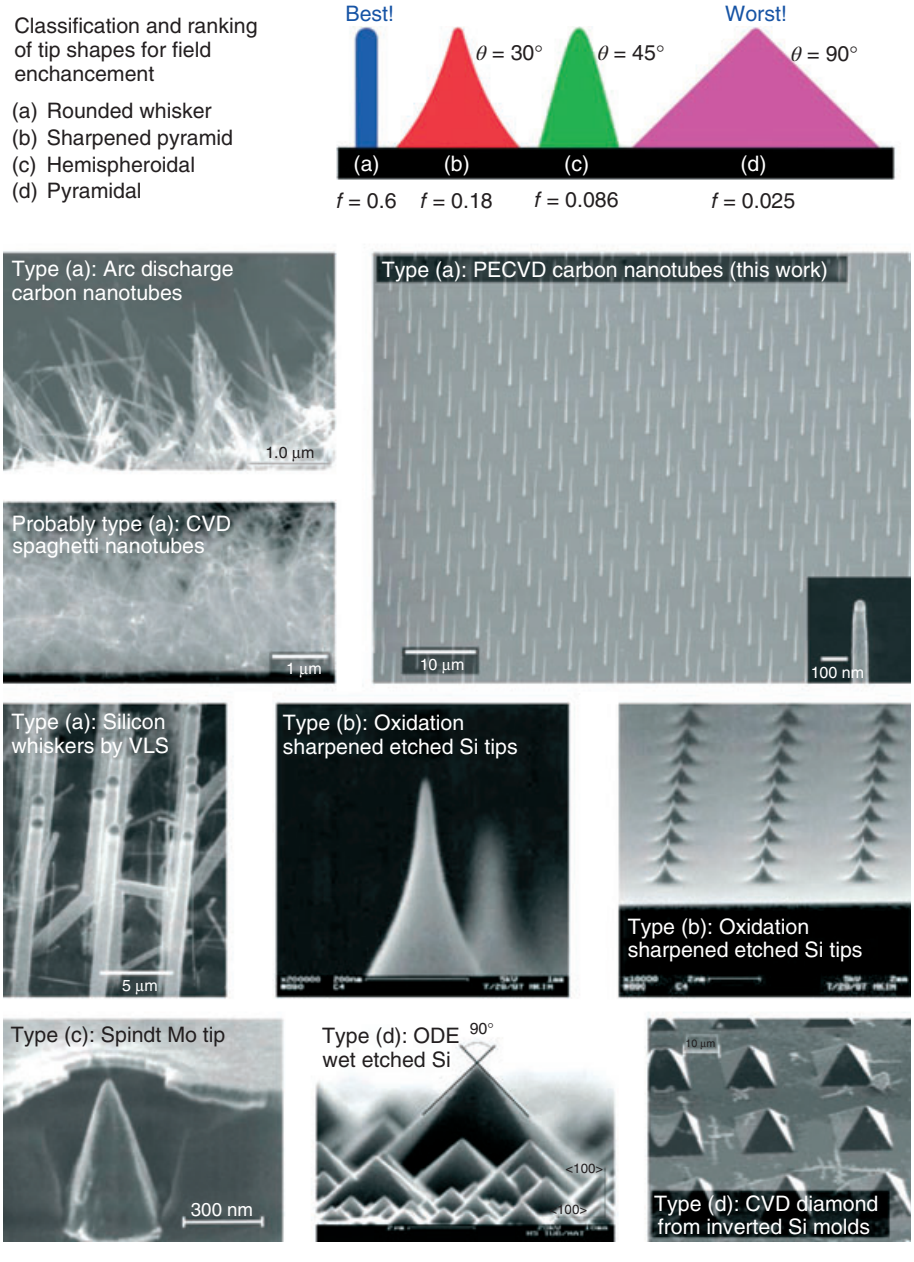

Figure 6 The Utsumi [15] tip-shape classification and ranking [38]: (a) an ideal rounded whisker, (b) sharpened pyramid, (c) hemispheroidal, and (d) pyramidal [67–72]. *Source*: Reproduced with permission from Ref. 5. © Royal Society of Chemistry, 2004

Handbook of Digital Imaging, Online © 2015 John Wiley & Sons, Ltd.
This article is © 2015 John Wiley & Sons, Ltd.
This article was published in the *Handbook of Digital Imaging* in 2015 by John Wiley & Sons, Ltd.
DOI: 10.1002/9781118798706.hdi023

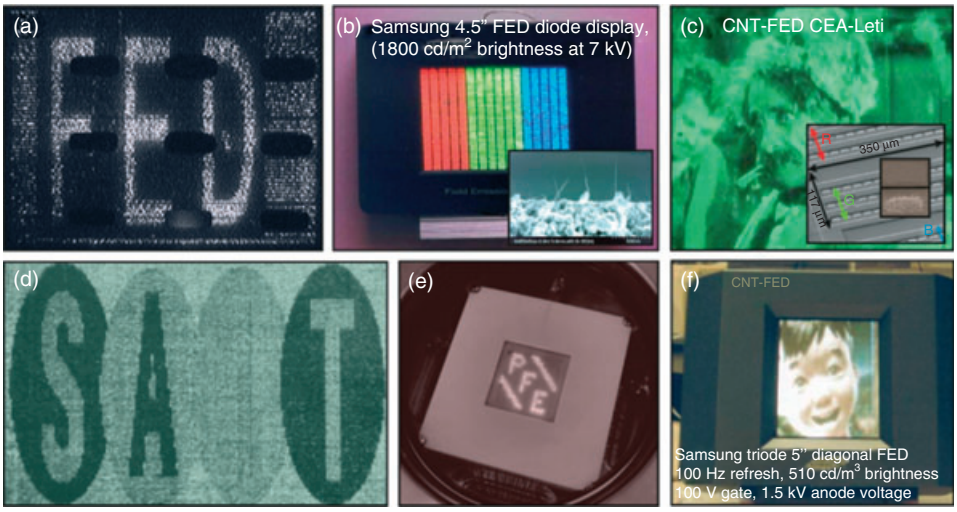

Figure 7 Next-generation nanomaterials-based FEDs. (a) A 2.55-in. fully vacuum-sealed FED (160 × 360 pixel) prototype by Motorola based on nitrogen-doped amorphous carbon emitters with a 45-V switching voltage [39, 53]. (b) A screen-printed carbon nanotube FED developed by Samsung SDI (1999) [75]. *Inset:* Cross-section scanning electron micrograph of the carbon nanotube field emitters [75]. A 30-in. diagonal version of the technology was reported to be near completion in 2004 (Samsung Display Technology. Courtesy of Y. Choi). (c) Monochramitc, 350-µm pixel, CNT-FED developed by CEA-Leti. A full color, 600-µm pixel, display has also been reported (Courtesy of CEA-LITEN, http://issuu.com/phantoms_foundation/docs/e_nano_newsletter_issue20_21/24). (d) Samsung Advanced Institute of Technologies carbon nanotube-based 9-in./576 × 240 pixel thick film display [39, 76] (Courtesy of J. M. Kim, SAIT). (d) Printed Field Emitters (PFE), Ltd., addressable display. The emitters are formed by conductive particles in an insulating matrix [39]. (f) A video running 5-in. carbon nanotube FED by Samsung Advanced Institute of Technology (SAIT), operating at a gate potential of 100 V, an anode bias of 1.5 kV, and a drive frequency of 100 Hz [77]. *Source*: Reproduced with permission from Ref. 5. © Allied Publishing LLC, 2004

both monochromatic and full color FED where the emitters were formed from directly chemical vapor deposited pixel arrays of 20 µm spaghetti-like CNT forests (Figure 7c). The inset of Figure 7c shows scanning electron micrographs (SEMs) of the patterned catalyst, synthesized spaghetti-like CNTs, and a subset of the pixel array.

CNT thin films have been shown to make excellent field emitters, and most display prototypes use thin films of CNTs that are in spaghetti morphologies. Although the spaghetti-type networks function adequately well in displays, Nilsson *et al*. [79], Groning *et al*. [80], and Bonard *et al*. [81], however, all showed that such close packing densities introduce significant nearest-neighbor electrostatic shielding effects (Figure 8), which reduces the films effective field enhancement factor. Moreover, spatially resolved scanning field emission mapping also showed that such spaghetti networks have broad β distributions – a product of the rough films. Thus, such displays turn on at very low voltages but are largely unstable and have poor lifetimes. To fully exploit the exceptionally high field enhancement of each nanotube, vertically aligned arrays of nanotubes [82–84] are necessary with a pitch equal to approximately twice their height, as illustrated in Figure 9, which simultaneously have narrow distribution in β,

Handbook of Digital Imaging, Online © 2015 John Wiley & Sons, Ltd.
This article is © 2015 John Wiley & Sons, Ltd.
This article was published in the *Handbook of Digital Imaging* in 2015 by John Wiley & Sons, Ltd.
DOI: 10.1002/9781118798706.hdi023

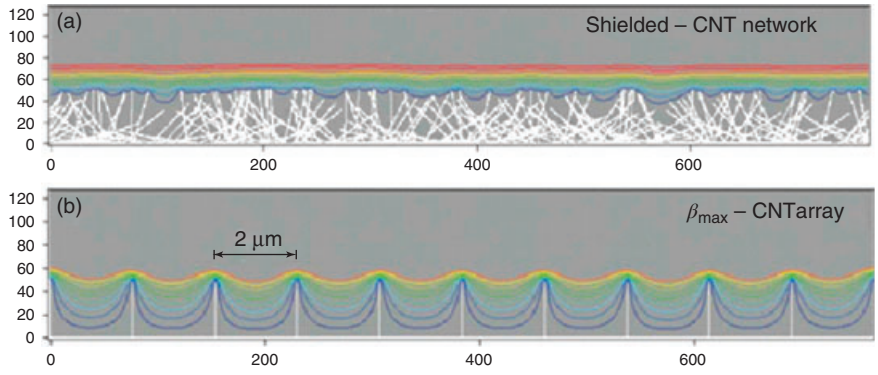

Figure 8 Simulated electrostatic screening interactions. (a) Significant screening occurring in dense unaligned CNT films, and (b) maximized aligned-CNT packing density simultaneously achieving high current densities with minimized shielding effects [5]. *Source*: Reproduced with permission from Ref. 5. © Allied Publishing LLC, 2004

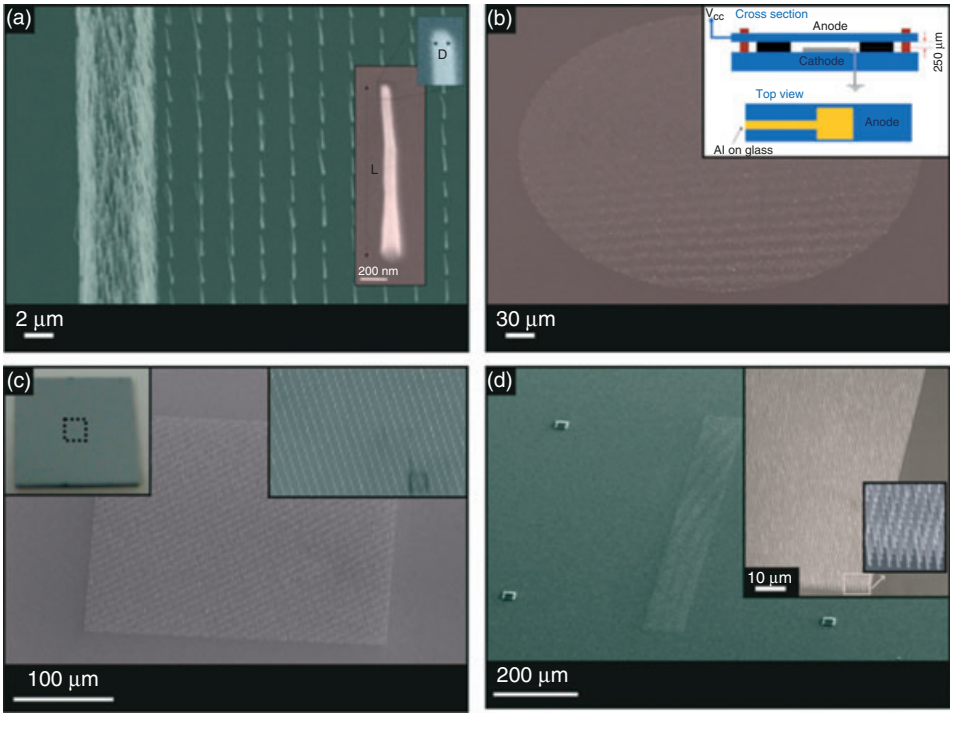

Figure 9 Various periodic carbon nanotube arrays synthesized by plasma-enhanced chemical vapor deposition [66, 85]. *Inset*: a typical field emission setup

Handbook of Digital Imaging, Online © 2015 John Wiley & Sons, Ltd.
This article is © 2015 John Wiley & Sons, Ltd.
This article was published in the *Handbook of Digital Imaging* in 2015 by John Wiley & Sons, Ltd.
DOI: 10.1002/9781118798706.hdi023

which enhances display longevity. In 2006, Motorola was the first to achieve this in its published work on the nanoemissive large area high definition prototype displays using *in-situ* chemical vapor deposited and selectively positioned vertically aligned CNTs on glass substrates but has since discontinued all FED development [86, 87].

The various CNT-based FED prototypes have shown promise. Indeed, comparable pixel-to-pixel nonuniformity (5%) to those of LCDs (3%) and CRTs (2%) has been demonstrated. Sony's Field Emission Displays, Inc. – a spin-off entity based on the intellectual assets acquired from Nanotechnoliges, Inc., and entirely focused on FED production – was charged with the continued development of their field emission displays. However, Sony closed down its FED sector in 2009 in a company-wide back-off from FED technologies. AU Optronic from Taiwan acquired assets that included patents, various intellectual property rights, processing equipment, and materials from Japan-based FET, which was 40% owned by Sony, Corp. AU Optronic has maintained a concerted effort to develop the technology but has not as yet commented on planned mass production.

In addition to the nanostructured carbon field emitting arrays (FEAs), other promising FEAs have been developed based on transfer mold fabrication methods [88–96]. The main limiting features of FEDs are the emission current uniformity and tip sharpening. Low turn-on voltages have been deemed the most important parameters for the successful commercialization of FEDs. Defects in the phosphor coatings, which are caused by material and deposition nonuniformities, and high current fluctuations across large area FEAs provide another major challenge. To ensure high image quality, current fluctuations should be less than $\pm 1\%$. The emission current fluctuation of conventional FEAs, including CNT-based FEAs with and without ballast layers, are usually somewhere between $\pm 5\%$ and $\pm 100\%$ [93, 94], although, recently, stabilities as low as $\pm 0.68\%$ have been reported for SOI-ballasted CNT emitters [3].

Various transfer mold fabrication methods have been developed to fulfill the requirements previously stipulated and have taken into consideration the emitter material, uniformity, and reproducibility. A key feature of the mold techniques developed is the ability to form extremely sharp tips with a radius <10 nm, good uniformity, low emission current fluctuations (± 0.7–4.3%), and the use of a low work function emitter [65–73]. One of the more common transfer mold methods uses Si mold substrates, as illustrated in Figure 10a [95]. A Si(100) substrate is anisotropically etched, through a thermally oxidized SiO_2 hard mask, using 30% aqueous KOH, to form pyramidal holes with very sharp vertices. This forms a master "mold." These masters can fabricate many similar transfer mold FEAs in a uniform and reproducible manner [92, 93]. The width of the openings usually ranges from 36 nm to 1.6 μm. The Si molds are thermally oxidized to form a low leakage, emitter-to-gate dielectric layer. The resistivity of this dielectric is two to three times that of directly physical vapor deposited SiO_2 insulators. Another important feature of the thermal oxidation process is that, during the SiO_2 growth, the mold sidewalls become increasingly convex, which improves the emitters' geometry. Emitter materials are deposited onto the SiO_2 layer by physical vapor processes, such as sputtering, CVD, and electroplating, to fill the mold. The convex shape of the Si mold sharpens the emitter tips at the bottom of the mold. The emitter material is then bonded to a glass substrate via electrostatic anodic bonding [97]. The Si mold is subsequently removed using an anisotropic wet etch, using tetramethyl ammonium hydroxide, for example. The engineered emitter profiles are transferred, with high fidelity, from the Si master mold. Because the emitter tips are sharpened during the transfer process, there is little need for postprocessing sharpening. In order to introduce gated functionality to the transfer mold

Handbook of Digital Imaging, Online © 2015 John Wiley & Sons, Ltd.
This article is © 2015 John Wiley & Sons, Ltd.
This article was published in the *Handbook of Digital Imaging* in 2015 by John Wiley & Sons, Ltd.
DOI: 10.1002/9781118798706.hdi023

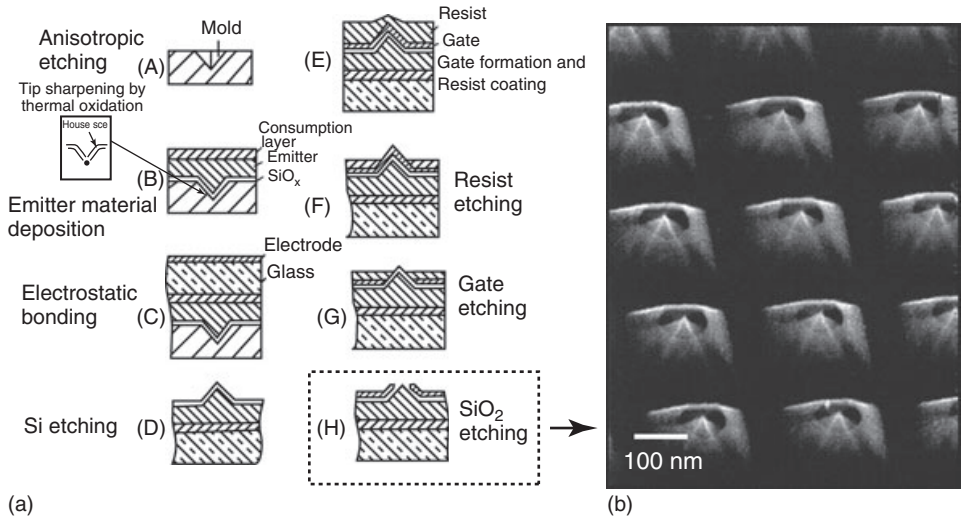

Figure 10 Transfer mold field emission arrays. (a) Fabrication process using Si mold substrates and metallic emitters. (b) A scanning electron micrograph of a gated transfer mold Mo FEA [92]

FEAs, a gate layer and resist layer can be coated on the SiO_2 layer. The thin resist layer is dry etched in oxygen plasma to reveal the tips of the coated emitters. Finally, wet etching of both the gate and the oxide results in submicron openings in the gated transfer mold FEAs.

Figure 10b shows an SEM of a Mo-gated transfer mold FEA. Emitter base lengths can be accurately controlled from 36 nm to 3 μm. The emitters turn on at voltages as low as 7 V [89]. In many FEDs, the turn-on potential is perhaps more important than the turn-on electric field as a figure of merit. The turn-on potential directly relates to arc-induced defects, which are caused by high fluctuation of emission current and high driving voltages. In addition, low turn-on voltages avoid ionization of remnant gases, which induce deterioration of the emitting arrays. Conversely, the true values of the electric fields, that is F_{local}, cannot be easily measured during experimentation as the electric field is not constant in the vacuum cavity between the FEA and counter electrode. An important point to note is that even atomically sharp FEAs cannot reduce the turn-on voltage lower than the work function of the emitting material. Note also that the turn-on electric fields are dependent on the distance between the emitter and the extraction electrodes. Before the turn-on fields of different emitters can be critically compared, the differences in the electrode geometry must be considered accordingly. Furthermore, strictly speaking, the turn-on voltage cannot be calculated directly from the turn-on electric field and the electrode distance. According to the quantum mechanical theory, even under exceptionally large electric fields ascribed to nanometer-scale tip radii and nanometer-scale electrode separation, in order to excite electrons from the Fermi level to the vacuum level, they must acquire energy equivalent to that between the Fermi level and the vacuum level, that is, the work function of the emitter materials. Thus, inherently, the turn-on voltages must be larger than the work function of any given emitter. For example, even if the turn-on electric field of the FEA using one material, whose work function is 5.0 eV, is as low as 1 V/μm at an electrode distance of 1 mm (through the application of 1 kV, say), the turn-on electric field should increase from

Handbook of Digital Imaging, Online © 2015 John Wiley & Sons, Ltd.
This article is © 2015 John Wiley & Sons, Ltd.
This article was published in the *Handbook of Digital Imaging* in 2015 by John Wiley & Sons, Ltd.
DOI: 10.1002/9781118798706.hdi023

1 V/μm and must be higher than 50 V/μm at an electrode distance of 0.1 μm. This is because the extraction voltage must be higher than 5.0 V, that is, the work function of the emitter. Usually, the turn-on electric fields measured at 1–2 mm electrode distance can be maintained down to electrode separations of 100–300 μm. However, the turn-on electric fields gradually increase at electrode separations less than 100–300 μm and significantly increase at separations less than 10–30 μm. Thus, in order to compare and evaluate the performance of various FEAs, the electrode distance must be mentioned and considered. Thus, for the work function of Mo (4.5 eV), the turn-on voltage of 7.0 V is close to the theoretical minimum value of 4.5 V. The approximate turn-on field is 17.5 V/μm, for a 0.4-μm gate-emitter separation. Moreover, the turn-on voltage is less than the ionization potential (12–20 V) of the residual gas.

The emission currents in such devices have been shown to fluctuate by ±4.3–7.0% and ±0.7% for the transfer mold Mo FEAs, for emitter base lengths of 1.6 μm, with and without resistive ballast layers [90], respectively, which are some of the lowest values reported. One of the main advantages of the transfer mold method is that the emitter material can be changed easily. The fluctuation in the emission currents of transfer mold Ni, TiN, and *a*-C FEAs without resistive ballasts are ±2% [93], ±2.5% [94], and ±1.7% [96], respectively. In the case of miniaturized transfer mold Mo FEAs, with emitter base length of 36 nm, without resistive ballasts, the emission current fluctuation is reduced from ±7% (1.6 μm emitter base length) to ±1.6% [90, 95]. By adding resistive layers, changing the emitter materials and miniaturizing the device reliably, large area FEAs can be attained that offer a viable means toward the possible realization of FEDs in the future.

The commercialization and technological history of electron emission displays has been no-less than turbulent. Taking over 50 years from inception – based on the ground breaking work of Fowler, Nordheim, Oppenheimer, and Baker – to partial commercialization, a wide range of emitting technologies and materials have been developed by many companies, including, but certainly not limited to, Futaba, Motorola, Raytheon, Candescent, Samsung, Sony, Micron Display, and AU Optronics. Although many of these international conglomerates have stated ongoing research efforts, the future of electron emission displays is still unclear. Nonetheless, the basic concept has produced significant interest and generated substantial amounts of know-how and fundamental science that, in the early 2000s, resulted in the conception of a new derivative, the surface emission display (SED) [88, 98–101], which may yet turn out to be the next ubiquitous display technology.

4 Surface-Conduction Electron-Emitter Displays

Surface-conduction electron-emitter displays (SEDs) may quite possibly offer a platform for the next generation of field emission based display technologies. SEDs are similar to FEDs in a number of critical ways but differ primarily in the details of the emitter design. Figure 11 show the basic structure of a SED and the structure of a single surface-conduction electron emitter (SCE). The SED primarily consists of planar electrodes and spacers that maintain the interelectrode separation. The distinctive feature of the SED is the use of the SCEs on the cathode plate. Compared to FEDs and other field emitting technologies, SEDs are distinct as the SCE are lateral emitters rather than vertical protrusions or other longitudinal type emitters. Electrons are emitted parallel to the insulating substrate (typically quartz or glass) and move principally toward the gate electrode, with minor perpendicular deviations in the beam trajectory toward the biased anode. After colliding with the gate electrode, some of the electrons

Handbook of Digital Imaging, Online © 2015 John Wiley & Sons, Ltd.
This article is © 2015 John Wiley & Sons, Ltd.
This article was published in the *Handbook of Digital Imaging* in 2015 by John Wiley & Sons, Ltd.
DOI: 10.1002/9781118798706.hdi023

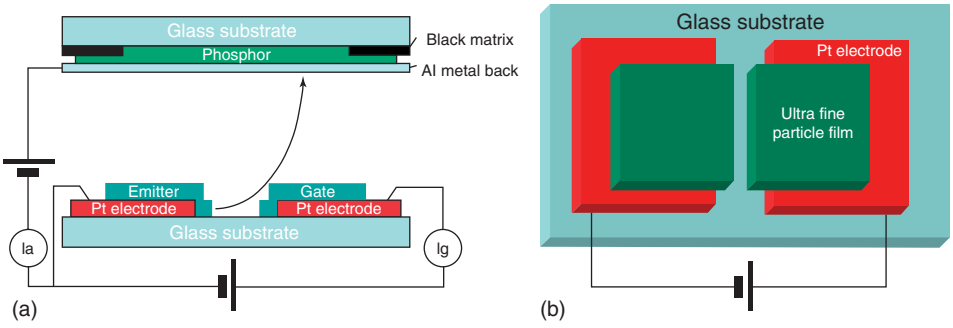

Figure 11 (a) Structure of a surface-conduction electron-emitter display; (b) structure of a surface-conduction electron emitter

are backscattered toward the anode, while the remaining electrons are efficiently absorbed by the gate.

There are a number of advantages to SCEs. Their simple structure, ease of manufacture, and low fabrication cost – by means of facile nanoimprinting techniques – are perhaps some of the most obvious. More importantly, however, is the fact that they require very low driving voltages, approximately one to two orders of magnitude less than those used in FEDs, owing to the tens of nanometers spacing between the cathode and the gate. SCE emitters are specifically interesting as they offer emission platforms that are simple to fabricate and well suited to large area flat panel displays (40–50 in.). Nevertheless, SCEs suffer from low electron efficiencies (1–3%) [65, 75, 78], defined as the ratio of the anode current to the gate current, in addition to nonconcentric biased electron trajectory, which forms an undesirable crescent-like pattern on the light emitting phosphor-coated anode [88, 101].

SEDs were based on an entirely novel technology though few practical displays have been reported to date. In the concluding section of this chapter, we discuss the fabrication and functionality of one such display. The typical fabrication process of an SCE is depicted in Figure 11a [96]. First, a pair of metallic (often Pt) electrodes is deposited onto polished glass substrates by physical vapor deposition. A 10-nm dielectric thin film is then deposited onto the electrodes by inkjet printing of ultrafine PdO nanoparticles [88]. Emitter formation is carried out by applying electric pulses, <10 $V_{p\text{-}p}$, to the particulate PdO thin film under vacuum. The PdO is reduced as a result of Joule heating. During the heating process, the Pd film contracts and sublimates along the diameter of the circular thin films such that a submicron gap is formed at their centers. A second electric pulse is then applied until the Pd film is completely divided into two sections, and the insulation, provided by the submicron gap, is maintained. Finally, an activation process is carried out to form a carbon nanogap within this submicron gap. Organic gases are introduced into the vacuum chamber of a thermal CVD system. Electric pulses, of approximately 20 V, are then applied across the submicron region, which instigates significant Joule heating by plasma and electron emission effects. The heating process thermally decomposes the hydrocarbon feedstock resulting in the deposition of carbon nanostructures. The carbon nanogap is produced directly on the Pd submicron gap, which functions as the cathode. Finally, a firing process, at 300°C under vacuum, completes the fabrication cycle.

Handbook of Digital Imaging, Online © 2015 John Wiley & Sons, Ltd.
This article is © 2015 John Wiley & Sons, Ltd.
This article was published in the *Handbook of Digital Imaging* in 2015 by John Wiley & Sons, Ltd.
DOI: 10.1002/9781118798706.hdi023

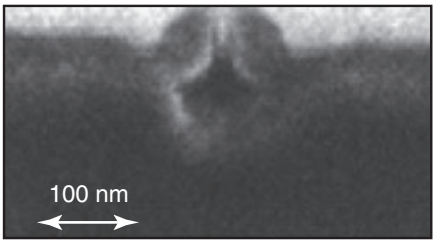

Figure 12 Cross-section scanning electron micrograph of a SCE carbon nanogap (scale bar: 100 nm) [88]

Figure 12 shows a cross-sectional SEM of a single SCE detailing the carbon nanogap [88]. The width of the nanogaps can be as narrow as 4–6 nm. The thickness is typically 30–50 nm. The width of the nanogaps can be accurately controlled by the pressure of the organic gases and the waveform of the pulsed voltage applied during the activation process.

Owing to the nanogap, the driving gate voltage can be as low as 14–22 V [65, 75, 78] for an anode bias of 10 kV. Such low driving potentials are helpful in mitigating deleterious arcing effects while concurrently reducing power consumption. Emission currents of up to 40 μA per emitter have been recorded, giving a current density as high as 3 A/cm^2, which is more than suitable for phosphor excitation in display applications [88]. Under such intense emission currents, the electron emission efficiency is around 3% [88].

Each pixel uses a pair of SCEs in order to engineer beam symmetry by overcoming the asymmetric-biased crescent electron trajectory. The trajectories of the emitted electrons have been calculated using a multiple electron scattering model of the gate. It is based on the initial energy of the emitted electrons as well the anode electric field, which is determined by the anode voltage and the interelectrode separation. The beam width is approximately 110 μm at an anode voltage of 10 kV, a gate voltage of 19 V, and an interelectrode separation of 1.7 mm [65, 78]. Prototype 36-in. SEDS have been fabricated with pixel widths of approximately 205 μm, assuming WXGA resolution, and the 110-μm beam spreading accounts for almost half the pixel [101]. Consequently, pairs of SCEs constitute single pixels where these dual beam emitter systems focus to a single phosphor RGB element without the need of any electromagnetic focusing electrodes. The crescent shaped twin-luminescent patterns have an interpattern separation of around 90 μm and demonstrate emission intensities of 400 cd/m^2.

SCE arrays are fabricated principally by inexpensive, facile, and highly controllable inkjet printing. Similarly, the scanning and signal bus matrices are formed through a printing method using metals dispersed in organic solvents. Sequential line scans are used to drive SEDs, as in the case of standard LCDs. Typical WXGA displays based on SED technology have (H)1280 × (RGB)3 × (V)768 pixels, which correspond to a pixel size of approximately 205 μm × 3 × 615 μm. Once the cathode plate has been formed, approximately 20 individual ceramic spacers are arranged on the printed interconnects of the cathode plate. Spacers are used to avoid induced degradation of the electron beam trajectory imparted by the biased anode. The anode plate consists of a phosphor screen, color filters, and a conductive Al back plane, as illustrated in Figure 11a. The RGB phosphors are surrounded by a so-called *black matrix*, fabricated from conductive nanoparticulate carbon black, which increases the optical contrast of the display. P22 phosphors, consisting of green (ZnS:Cu, Al) blue (ZnS:Ag, Cl), and red

Handbook of Digital Imaging, Online © 2015 John Wiley & Sons, Ltd.
This article is © 2015 John Wiley & Sons, Ltd.
This article was published in the *Handbook of Digital Imaging* in 2015 by John Wiley & Sons, Ltd.
DOI: 10.1002/9781118798706.hdi023

(Y_2O_2S:Eu) phosphors are used to obtain a similar color palette and range as those of traditional CRT displays. More exotic color filters are available to reduce diffuse reflectance, eliminating additional emission spectra to improve the fidelity of the RGB emitters, while also further widening the color range. The opening pattern of the black matrix is designed to reduce the diffuse reflectance and to match the crescent emission pattern from pixel pairs. Each opening in the carbon black matrix is octagonal with an open pixel area of 155 μm × 275 μm that matches the paired crescent pixel size. The ratio of the black matrix to the pixel opening is 31%, giving a diffuse reflectance of 4.5% [88, 101]. Additional luminescence peaks associated with the red phosphor ($\lambda < 600$ nm) are effectively reduced by the low transmittance of the red filter. SCEs can obtain RGB purities of 94% across a wide color gamut [101], similar in scope to the National Television Systems Committee color range in the International Commission on Illuminations chromaticity diagram.

The cathode and anode plates are sealed by frit glass and a low melting point metal. The sealed structure is of the order of 2.8 mm thick [101]. The typical thickness of a completed SED panel can be as low as 7.3 mm, of which nearly 25% accounts for the anode–cathode separation. Figure 13 shows a prototype 55-in. SED ((H)1920 × (RGB)3 × (V)1080). The display demonstrates an increased brightness (450 cd/m^2) compared with that of the 36-in. SED. High luminous efficiencies of 5–7 lm/W have also been achieved [101, 102]. Rapid response times of <1 ms, defined as the 10% luminance decay time, have also been reported [101], making the technology a viable candidate for next-generation display technologies.

SCEs operate in a similar way to traditional field emitters and, as a result, show highly nonlinear current–voltage characteristics [101] consistent with the Fowler–Nordheim field emission theory, as previously discussed. High contrast blacks are possible by exploiting the nonlinearity of these characteristics. As the emission current is very low at a scanning voltage of −9.5 V (off-state), the brightness is also low (<4 × 10^{-3} cd/m^2). However, the brightness

Figure 13 A prototype 55-in. SED manufactured consisting of (H)1920 × 3 × (V)1080 pixels. The display showed high brightness (450 cd/m^2) with high luminous efficacies of 5–7 lm/W and rapid response times of <1 ms (Courtesy of M. Nakamoto, CEATEC-Japan, 2006 with kind permission of SED Corp.)

Handbook of Digital Imaging, Online © 2015 John Wiley & Sons, Ltd.
This article is © 2015 John Wiley & Sons, Ltd.
This article was published in the *Handbook of Digital Imaging* in 2015 by John Wiley & Sons, Ltd.
DOI: 10.1002/9781118798706.hdi023

reaches more than 400–450 cd/m^2 [101] at a scanning voltage of +9.4 V (on-state), which corresponds to a driving voltage of 18.9 V, resulting in a contrast ratio of 10^5:1 [101].

SEDs are superior to their CRT counterparts, in terms of focusability. Substantially finer images can be attained by virtue of the emitter design. The distance between the emitter and phosphor is typically of the order of millimeters. This significantly reduces the path length of the electron beam, thereby reducing possible beam divergence and consequent image blurring. The focusability of SEDs is uniform across the entire emitter population, even at the periphery of the screen, owing to the "fixed pixel"-type display. In contrast, the electron beam can be heavily distorted and can be difficult to magnetically focus at the display edges in CRT-based displays.

5 Summary

This chapter described the process of electron emission and showed how such quantum mechanical behavior can be used to engineer sharp, high brightness, good contrast ratio, flat panel displays. The main commercialization barriers of FEDs and SEDs have been identified and shown to include problems with processability, emitter longevity, vacuum lifetime, and stability allied to the costs incurred in supplanting the current state-of-the-art display technologies. Perhaps, the future of FEDs and SEDs will focus on the development of high end displays and those for use in harsh environments.

Acknowledgments

M. T. Cole and W. I. Milne wish to acknowledge the ongoing support of and collaboration with: Y. Zhang, C. Li, K. Qu, K. B. K. Teo, M. Mann, G. A. J. Amaratunga, P. Hiralal, D. Pribat, N. Rupesinghe, P. Legagneux, L. Gangloff, M. Chhowalla, E. Minoux, L. Hudanski, F. Peauger, N. de Jonge, D. Dieumgard, O. Groening, V. T. Binh, and V. Semet – without whom much of this work would not have been possible. We also wish to thank D. G. Hasko for fruitful discussions and experimental insight and to all those who contributed, past and present.

M. Nakamoto acknowledges his colleagues and students at Toshiba, Corp., Canon, Inc., SED, Corp., and Shizuoka University: T. Hasegawa, Y. Nakamura, K. Yamamoto, T. Oguchi, I. Nomura, K. Suzuki, K. Hatanaka, J. H. Moon, and W. Kurota. Special thanks are extended to K. Fukuma for his assistance in the research presented.

We express sincere apologies to all those individuals who have made contributions to the field whom, due to space constraints, we did not mention.

References

1. Shah, I. (1997) Field-emission displays. *Physics World*, **10**, 45–50.
2. Gomer, R. (1961) Field emission and field ionization. *Harvard Monographs in Applied Sciences*, **9**, 195.
3. Cole, M.T., Li, C., Zhang, Y., *et al.* (2012) Hot electron field emission *via* individually transistor-ballasted carbon nanotube arrays. *ACS Nano*, **6**, 3236–3242.
4. Jenkins, R.O. and Trodeen, W.G. (1965) in *Electron and Ion Emission from Solids In Solid-State Physics* (ed. L. Jacob), Routledge and Kegan Paul Ltd., London.
5. Milne, W.I., Teo, K.B.K., Amaratunga, G.A.J., *et al.* (2004) Carbon nanotubes as field emission sources. *Journal of Materials Chemistry*, **14**, 933–943.

Handbook of Digital Imaging, Online © 2015 John Wiley & Sons, Ltd.
This article is © 2015 John Wiley & Sons, Ltd.
This article was published in the *Handbook of Digital Imaging* in 2015 by John Wiley & Sons, Ltd.
DOI: 10.1002/9781118798706.hdi023

6. Forbes, R.G. (2006) Simple good approximations for the special elliptic functions in standard Fowler-Nordheim tunneling theory for a Schottky-Nordheim barrier. *Applied Physics Letters*, **89**, 1221–1223.
7. Murphy, E.L. and Good, R.H. (1956) Thermionic emission, field emission, and the transition region. *Physical Review*, **102**, 1464–1473.
8. Brodie, I. and Spindt, C.A. (1992) Vacuum microelectronics. *Advances in Electronics and Electron Physics*, **83**, 1–106.
9. Nation, J.A., Schachter, L., Mako, F.M., *et al.* (1999) Advances in cold cathode physics and technology. *Proceedings of the IEEE*, **87**, 865–889.
10. Lee, Y.H., Choi, C.H., Jang, Y.T., *et al.* (2002) Tungsten nanowires and their field electron emission properties. *Applied Physics Letters*, **81**, 745–747.
11. Rohrbach, F. (1971) CERN Report 71–28, http://slac.stanford.edu/cgi-wrap/getdoc/slac-pub-7684.pdf
12. Dresselhaus, M.S. and Avouris, P. (2001) Introduction to carbon materials research. *Carbon Nanotubes*, **80**, 1–9.
13. Fowler, R.H. and Nordheim, L. (1928) Electron emission in intense electric fields. *Proceedings of the Royal Society of London Series a-Containing Papers of a Mathematical and Physical Character*, **119**, 173–181.
14. Wu, J.W. and Mahan, G.D. (1983) Dynamic image potentials and field-emission. *Physical Review B*, **28**, 4839–4841.
15. Utsumi, T. (1991) Vacuum microelectronics: whats new and exciting? – keynote address. *IEEE Transactions on Electron Devices*, **38**, 2276–2283.
16. Richardson, O.W. (2003) *Thermionic Emission from Hot Bodies*, Wexford College Press, Aberdeen.
17. Guthrie, F. (1873) On a new relation between heat and electricity. *Proceedings of the Royal Society of London*, **21**, 168–169.
18. Francis, W., Zemansky, M.W., and Young, H.D. (1983) *University Physics*, Addison-Wesley, pp. 843–844.
19. Shoulders, K.R. (1961) Microelectronics using electron-beam-activated machining techniques, in *Advances in Computers*, vol. 2 (ed. F.L. Alt), Academic Press, New York, pp. 135–293.
20. Amaratunga, G. (2003) Watching the nanotube. *IEEE Spectrum*, **40**, 28–32.
21. Encyclopaedia Britannica, Inc. (2014) Today on Britannica, http://www.Britannica.Com (Ph/computers/cathode-ray-tube-crt-360037.Html) (accessed 29 January 2014).
22. Williams, B.F. and Simon, R.E. (1969) Electron emission from a cold-cathde gas p-n junction. *Applied Physics Letters*, **14**, 214.
23. Ke, S., Jae Young, L., Biyun, L., *et al.* (2010) Field Emission Properties of Atomically Sharp Tungsten Nanotip Arrays Fabricated by a Novel Nanocasting Method. Technical Digest of the 23rd International Vacuum Nanoelectronics Conference, pp. 205–206.
24. Xu, N.S., Chen, J., and Deng, S.Z. (2000) Physical origin of nonlinearity in the Fowler-Nordheim plot of field-induced emission from amorphous diamond films: thermionic emission to field emission. *Applied Physics Letters*, **76**, 2463–2465.
25. Cheng, T.C., Hsueh, H.T., Huang, W.J., *et al.* (2005) Measurement of field-emission properties of a single crystallized silicon emitter using scanning electronic microscopy. Microscopy of Semiconducting Materials, Springer, *Proceedings in Physics*, **107**, 351–354.
26. Amaratunga, G.A.J. and Silva, S.R.P. (1996) Nitrogen containing hydrogenated amorphous carbon for thin-film field emission cathodes. *Applied Physics Letters*, **68**, 2529–2531.
27. Satyanarayana, B.S., Hart, A., Milne, W.I., *et al.* (1997) Field emission from tetrahedral amorphous carbon. *Applied Physics Letters*, **71**, 1430–1432.
28. Okano, K., Koizumi, S., Silva, S.R.P., *et al.* (1996) Low-threshold cold cathodes made of nitrogen-doped chemical-vapour-deposited diamond. *Nature*, **381**, 140–141.
29. Musa, I., Munindrasdasa, D.A.I., Amaratunga, G.A.J., *et al.* (1998) Ultra-low-threshold field emission from conjugated polymers. *Nature*, **395**, 362–365.
30. Li, C., Zhang, Y., Mann, M., *et al.* (2010) Stable, self-ballasting field emission from zinc oxide nanowires grown on an array of vertically aligned carbon nanofibers. *Applied Physics Letters*, **96**, 143114–143117.
31. Teo, K.B.K., Chhowalla, M., Amaratunga, G.A.J., *et al.* (2002) Field emission from dense, sparse, and patterned arrays of carbon nanofibers. *Applied Physics Letters*, **80**, 2011–2013.
32. Baker, F.S., Williams, J., Osborn, A.R. (1972) Field-emission from carbon fibers – new electron source. *Nature*, **239**, 96–97.
33. Wang, C., Garcia, A., Ingram, D.C., *et al.* (1991) Cold field-emission from CVD diamond films observed in emission electron-microscopy. *Electronics Letters*, **27**, 1459–1461.

Handbook of Digital Imaging, Online © 2015 John Wiley & Sons, Ltd.
This article is © 2015 John Wiley & Sons, Ltd.
This article was published in the *Handbook of Digital Imaging* in 2015 by John Wiley & Sons, Ltd.
DOI: 10.1002/9781118798706.hdi023

34. Geis, M.W., Efremow, N.N., Woodhouse, J.D., *et al.* (1991) Diamond cold-cathode. *IEEE Electron Device Letters*, **12**, 456–459.
35. Djubua, B.C. and Chubun, N.N. (1991) Emission properties of spindt-type cold cathodes with different emission cone material. *IEEE Transactions on Electron Devices*, **38**, 2314–2316.
36. Hart J.A., Lenway S.A. and Murtha T. (1999) A History of Field Emission Displays.
37. Bernhardt, A.F., Contolini, R.J., Jankowski, A.F., *et al.* (2000) Arrays of field emission cathode structures with sub-300 nm gates. *Journal of Vacuum Science and Technology B*, **18**, 1212–1215.
38. Milne, W.I., Teo, K.B.K., Mann, M., *et al.* (2006) Carbon nanotubes as electron sources. *Physica Status Solidi A*, **203**, 1058–1063.
39. Talin, A.A., Dean, K.A., and Jaskie, J.E. (2001) Field emission displays: a critical review. *Solid State Electronics*, **45**, 963–976.
40. Sonys Field emission company want to roll out 60 inch FED-TV.
41. Himpsel, F.J., Knapp, J.A., VanVechten, J.A., *et al.* (1979) Quantum photoyield of diamond(111) 151 Agnstrom stable negative-affinity emitter. *Physical Review B*, **20**, 624.
42. van der Weide, J., Zhang, Z., Baumann, P.K., *et al.* (1994) Negative-electron-affinity effects on the diamond(100) surface. *Physical Review B*, **50**, 5803–5806.
43. Bandis, C. and Pate, B.B. (1995) Photoelectric emission from negative-electron-affinity diamond(111) surfaces: Exciton breakup versus conduction-band emission. *Physical Review B*, **52**, 12056–12071.
44. Gerber, J., Robertson, J., Sattel, S., *et al.* (1996) Role of surface diffusion processes during bias-enhanced nucleation of diamond on Si. *Diamond and Related Materials*, **5**, 261–265.
45. Gilkes, K.W.R., Sands, H.S., Batchelder, D.N., *et al.* (1998) Direct observation of sp(3) bonding in tetrahedral amorphous carbon UV Raman spectroscopy. *Journal of Non-Crystaline Solids*, **227**, 612–616.
46. Mann, M., Teo, K.B.K., and Milne, W.I. (2008) Carbon nanotubes as electron sources, *Materials Science Foundation*.
47. Shim, J.Y., Baik, H.K., and Song, K.M. (2000) Effect of nondiamond carbon on electron transport path of field-emitted electrons from undoped polycrystalline diamond films. *Journal of Vacuum Science and Technology A*, **18**, 1977–1982.
48. Talin, A.A., Felter, T.E., Friedmann, T.A., *et al.* (1996) Electron field emission from amorphous tetrahedrally bonded carbon films. *Journal of Vacuum Science and Technology A*, **14**, 1719–1722.
49. Teo, K.B.K., Rodil, S.E., Tsai, J.T.H., *et al.* (2001) Effect of graphitic inclusions on the optical gap of tetrahedral amorphous carbon films. *Journal of Applied Physics*, **89**, 3706–3710.
50. Zhu, W., Kochanski, G.P., Jin, S., *et al.* (1995) Defect-enhanced electron field-emission from chemical-vapor-deposited diamond. *Journal of Applied Physics*, **78**, 2707–2711.
51. Robertson, J. (1999) Mechanisms of electron field emission from diamond, diamond-like carbon, and nanostructured carbon. *Journal of Vacuum Science and Technology B*, **17**, 659–665.
52. Amaratunga, G.A.J., Baxendale, M., Rupesinghe, N., *et al.* (1999) Field emission from a new form of thin film amorphous carbon having nanoparticle inclusions and carbon nanotubes. *New Diamond Frontiers in Carbon Technology*, **9**, 31–51.
53. Talina, A.A., Chalamalaa, B., Colla, B.F., *et al.* (1998) Development of field emission flat panel displays at Motorola. *Materials Research Society*, **508**.
54. Dean, K.A., Chalamala, B.R., Coll, B.F., *et al.* (2002) Carbon nanotube field emission electron sources. *New Diamond Frontiers in Carbon Technology*, **12**, 165–180.
55. Jaskie, J.E. (1996) Diamond-based field-emission displays. *MRS Bulletin*, **21**, 59–64.
56. Iijima, S. (1991) Helical microtubules of graphitic carbon. *Nature*, **354**, 56–58.
57. Hutchison, J.L., Kiselev, N.A., Krinichnaya, E.P., *et al.* (2001) Double-walled carbon nanotubes fabricated by a hydrogen arc discharge method. *Carbon*, **39**, 761–770.
58. Shi, Z.J., Lian, Y.F., Zhou, X.H., *et al.* (1999) Mass-production of single-wall carbon nanotubes by arc discharge method. *Carbon*, **37**, 1449–1453.
59. Thess, A., Lee, R., Nikolaev, P., *et al.* (1996) Crystalline ropes of metallic carbon nanotubes. *Science*, **273**, 483–487.
60. Scott, C.D., Arepalli, S., Nikolaev, P., *et al.* (2001) Growth mechanisms for single-wall carbon nanotubes in a laser-ablation process. *Applied Physics A*, **72**, 573–580.
61. Yudasaka, M., Yamada, R., Sensui, N., *et al.* (1999) Mechanism of the effect of NiCo, Ni and Co catalysts on the yield of single-wall carbon nanotubes formed by pulsed Nd : YAG laser ablation. *Journal of Physical Chemistry B*, **103**, 6224–6229.

Handbook of Digital Imaging, Online © 2015 John Wiley & Sons, Ltd.
This article is © 2015 John Wiley & Sons, Ltd.
This article was published in the *Handbook of Digital Imaging* in 2015 by John Wiley & Sons, Ltd.
DOI: 10.1002/9781118798706.hdi023

62. Cheol, J.L., Jeunghee, P., Yoon, H., *et al.* (2001) Temperature effect on the growth of carbon nanotubes using thermal chemical vapor deposition. *Chemical Physics Letters*, **343**, 33–38.
63. Choi, G.S., Cho, Y.S., Hong, S.Y., *et al.* (2002) Carbon nanotubes synthesized by Ni-assisted atmospheric pressure thermal chemical vapor deposition. *Journal of Applied Physics*, **91**, 3847–3854.
64. Chhowalla, M., Teo, K.B.K., Ducati, C., *et al.* (2001) Growth process conditions of vertically aligned carbon nanotubes using plasma enhanced chemical vapor deposition. *Journal of Applied Physics*, **90**, 5308–5317.
65. Hofmann, S., Ducati, C., Robertson, J., *et al.* (2003) Low-temperature growth of carbon nanotubes by plasma-enhanced chemical vapor deposition. *Applied Physics Letters*, **83**, 135–137.
66. Teo, K.B.K., Lee, S.B., Chhowalla, M., *et al.* (2003) Plasma enhanced chemical vapour deposition carbon nanotubes/nanofibres - how uniform do they grow? *Nanotechnology*, **14**, 204–211.
67. Wang, Q.H., Corrigan, T.D., Dai, J.Y., *et al.* (1997) Field emission from nanotube bundle emitters at low fields. *Applied Physics Letters*, **70**, 3308–3310.
68. Lee, S.B., Teh, A.S., Teo, K.B.K., *et al.* (2003) Fabrication of carbon nanotube lateral field emitters. *Nanotechnology*, **14**, 192–195.
69. Givargizov, E.I. (1993) Ultrasharp tips for field-emission applications prepared by the vapor liquid solid growth technique. *Journal of Vacuum Science and Technology B*, **11**, 449–453.
70. Meng, D., Han, K., and Akinwande, A.I. (2000) Highly uniform and low turn-on voltage Si field emitter arrays fabricated using chemical mechanical polishing. *IEEE Electron Device Letters*, **21**, 66–69.
71. Schroder, H., Obermeier, E., and Steckenborn, A. (1999) Micropyramidal hillocks on KOH etched {100} silicon surfaces: formation, prevention and removal. *Journal of Micromechanics and Microengineering*, **9**, 139–145.
72. Kang, W.P., Wisitsora-at, A., Davidson, J.L., *et al.* (1998) Micropattern-gated diamond field emitter array. *Journal of Vacuum Science and Technology B*, **16**, 732–735.
73. Purcell, S.T., Vincent, P., Journet, C., *et al.* (2002) Hot nanotubes: stable heating of individual multiwall carbon nanotubes to 2000 K induced by the field-emission current. *Physics Review Letters*, **88**, 105502/1–105502/4.
74. Wei, Y., Xie, C., Dean, K.A., *et al.* (2001) Stability of carbon nanotubes under electric field studied by scanning electron microscopy. *Applied Physics Letters*, **79**, 4527–4529.
75. Choi, W.B., Chung, D.S., Kang, J.H., *et al.* (1999) Fully sealed, high-brightness carbon-nanotube field-emission display. *Applied Physics Letters*, **75**, 3129–3131.
76. Uemura, S. (2002) Carbon Nanotube Field Emission Display. *Perspectives of Fullerene Nanotechnology*, pp. 57–65, http://link.springer.com/chapter/10.1007%2F0-306-47621-5_6) .
77. Chung, D.S., Park, S.H., Lee, H.W., *et al.* (2002) Carbon nanotube electron emitters with a gated structure using backside exposure processes. *Applied Physics Letters*, **80**, 4045–4047.
78. Kim J.M. (July 2003) Nanotube 2003 Conference.
79. Nilsson, L., Groening, O., Emmenegger, C., *et al.* (2000) Scanning field emission from patterned carbon nanotube films. *Applied Physics Letters*, **76**, 2071–2073.
80. Groening, O., Kuttel, O.M., Emmenegger, C., *et al.* (2000) Field emission properties of carbon nanotubes. *Journal of Vacuum Science and Technology B*, **18**, 665–678.
81. Bonard, J.M., Stockli, T., Noury, O., *et al.* (2001) Field emission from cylindrical carbon nanotube cathodes: possibilities for luminescent tubes. *Applied Physics Letters*, **78**, 2775–2777.
82. Teo, K.B.K., Chhowalla, M., Amaratunga, G.A.J., *et al.* (2003) Fabrication and electrical characteristics of carbon nanotube-based microcathodes for use in a parallel electron-beam lithography system. *Journal of Vacuum Science and Technology B*, **21**, 693–697.
83. Teo, K.B.K., Chhowalla, M., Amaratunga, G.A.J., *et al.* (2001) Uniform patterned growth of carbon nanotubes without surface carbon. *Applied Physics Letters*, **79**, 1534–1536.
84. Pirio, G., Legagneux, P., Pribat, D., *et al.* (2002) Fabrication and electrical characteristics of carbon nanotube field emission microcathodes with an integrated gate electrode. *Nanotechnology*, **13**, 1–4.
85. Cole, M.T., Mann, M., Li, C., *et al.* (2011) *Novel Nanostructured Carbon Nanotube Electron Sources.* International Conference on Materials for Advanced Technologies.
86. Coll, B.F., Dean, K.A., Howard, E., *et al.* (2006) Nano-emissive display technology for large-area HDTV. *Journal of the Society for Information Display*, **14**, 477–485.
87. Coll, B.F., Dean, K.A., Howard, E., *et al.* (2005) *Color Nano Emissive Displays for Large Area HD TV*. Technical Digest of the 18th International Vacuum Nanoelectronics Conference.
88. Yamamoto, K., Nomura, I., Yamazaki, K., *et al.* (2005) *Fabrication and Characterization of Surface Conduction Electron Emitters*. Technical Digest of 2005 International Symposium of Society for Information Display.

Handbook of Digital Imaging, Online © 2015 John Wiley & Sons, Ltd.
This article is © 2015 John Wiley & Sons, Ltd.
This article was published in the *Handbook of Digital Imaging* in 2015 by John Wiley & Sons, Ltd.
DOI: 10.1002/9781118798706.hdi023

89. Nakamoto, M., Hasegawa, T., Ono, T., *et al.* (1996) *Low Operation Voltage Field Emitter Arrays Using Low Work Function Materials Fabricated by Transfer Mold Technique*. Technical Digest of the 42nd IEEE International Electron Devices Meeting.
90. Nakamoto, M., Hasegawa, T., and Fukuda, K. (1997) *Uniform, Stable and High Integrated Field Emitter Arrays for High Performance Displays and Vacuum Microelectronic Switching Devices*. Technical Digest of the 43rd IEEE International Electron Devices Meeting.
91. Nakamoto, M. and Fukuda, K. (2002) Field electron emission from LaB6 and TiN emitter arrays fabricated by transfer mold technique. *Applied Surface Science*, **202**, 3611–3615.
92. Nakamoto, M. and Fukuda, K. (2003) Highly integrated field emitter arays fabricated by transfer mold technique. *Japanese Journal of Applied Physics*, **42**, 3611–3615.
93. Nakamoto, M., Moon, J., and Shiratori, K. (2010) Low work function nanometer-order controlled transfer mold field-emitter arrays. *Journal of Vacuum Science and Technology B*, **28**, C2B1–C2B4.
94. Nakamoto, M. and Moon, J. (2011) Suitability of low-work-function titanium nitride coated transfer mold field emitter arrays for harsh environment applications. *Journal of Vacuum Science and Technology B*, **29**, 02B111–02B115.
95. Nakamoto, M., Moon, J., and Kurota, W. (2011) *Extremely Stable, Low Operation Voltage and 36 nm Base Length Transfer Mold Field Emitter Arrays*. Technical Digest of the 24th International Vacuum Nanoelectronics Conference.
96. Nakamoto, M. and Moon, M. (2011) Extremely stable and low operation voltage transfer mold amorphous carbon field emitter arrays. *Proceedings of the 21st International Display Research Conference*, S9.2.
97. Wallis, G. and Pomerantz, D.I. (1969) Field assisted glass-metal sealing. *Journal of Applied Physics*, **40**, 3946–3949.
98. Yamaguchi, E., Sakai, K., Nomura, I., *et al.* (1997) A 10-in. surface-conduction electron-emitter display. *Journal of Society for Information Display*, **5**, 345–348.
99. Asai, A., Okuda, M., Matsutani, S., *et al.* (1997) *Multiple-Scattering Model of Surface-Conduction Electron Emitters*. Technical Digest of 1997 International Symposium of Society for Information Display.
100. Okuda, M., Matsutani, S., Asai, A., *et al.* (1998) *Electron Trajectory Analysis of Surface Conduction Electron Emitter Displays (SEDs)*. Technical Digest of 1998 International Symposium of Society for Information Display.
101. Oguchi, T., Yamaguchi, E., Sasaki, K., *et al.* (2005) *A 36-Inch Surface-Conduction Electron-Emitter Display*. Technical Digest of 2005 International Symposium of Society for Information Display.
102. Corporation, S. (2006) Demonstration of 55 in. Sed prototype, *CEATEC*.

Handbook of Digital Imaging, Online © 2015 John Wiley & Sons, Ltd.
This article is © 2015 John Wiley & Sons, Ltd.
This article was published in the *Handbook of Digital Imaging* in 2015 by John Wiley & Sons, Ltd.
DOI: 10.1002/9781118798706.hdi023